Low temperature rate coefficients for vibrational relaxation of 3Σ+u Rb2 molecules by 3He and 4He atoms

Alexandra Viel, Jean-Michel Launay

Low Temperature Rate Coefficients for Vibrational Relaxation of $^3\Sigma_u^+$ Rb_2 Molecules by ^{3}He and ^{4}He Atoms

Alexandra Viel* and Jean-Michel Launay*

Institut de Physique de Rennes, UMR 6251

CNRS & Université de Rennes 1,

F-35042 Rennes, France

E-mail: alexandra.viel@univ-rennes1.fr; jean-michel.launay@univ-rennes1.fr

KEYWORDS: quantum dynamics, collisions, bound-states, bosons and fermions

May 15, 2014

Abstract

We present quantum scattering calculations of ^{4}He and ^{3}He colliding with $^{87}Rb_2$. For both helium isotopes, the elastic and inelastic rate coefficients are strongly influenced by the $J = 1$ partial wave. For the lighter isotope a strong resonance feature of the $J = 1$ partial wave is responsible for an extremely efficient vibrational relaxation process. We also perform bound-state calculations of the Rb_2He complex for even Rb permutation symmetry and non-zero total angular momentum. The global Rb_2He $^3\Sigma_u^+$ potential energy surface used supports four bound states for ^{4}He and a single one for ^{3}He. We propose an analysis of the $^{87}Rb_2{}^4$He spectrum separating the contributions of Rb_2 rotation and helium motion.

*To whom correspondence should be addressed

Introduction

In recent years, the interest in producing dense samples of cold molecules as well as in detailed studies of reactions and collisions at cold and ultra-cold temperatures is rising.[1] In this context cold collisions of helium atoms with rubidium dimers in their high spin state have been studied.[2] A limitation of this former work[2] is the restriction of the calculation to the zero total angular momentum partial wave. Here we extend the scattering studies to non-zero total angular momentum using the three-dimensional potential energy surface for the lowest triplet state of the Rb_2He complex proposed by us.[2] Our study concerns the $v = 1, j = 0$ rovibrational state of $^{87}Rb_2$ as the initial state for collision with helium. All bound states of the complexes $Rb_2{}^3He$ and $Rb_2{}^4He$ with even Rb atoms permutation symmetry have also been determined. A new code that relies on a high order finite element method has been developed. It permits to compute both bound and scattering states.

The use of helium nanodroplets[3,4] enabled the production and spectroscopic studies of high spin alkali dimers and in particular rubidium dimers.[5] Indeed during the doping process the collision of two alkali atoms at the surface of the helium cluster leads preferentially to the high spin state dimer. Singlet state dimers are absent because of their large binding energy which induces a strong reduction of the cluster size by evaporation and most probably the detachment of the formed dimer.[5,6] Because of the very weak interaction between alkali dimers and helium atoms, the high spin alkali dimers stay on the surface of the helium droplet. Among the numerous works on Rb_2He_N, experimental and theoretical works have been dedicated to the understanding of the vibrational relaxation dynamics of such adsorbed weakly bound dimers. The vibrational dynamics of Rb_2 on an helium droplet has been the subject of femtosecond pump-probe experiments[7] from which a relaxation time of 2 ns has been extracted for the $1^3\Sigma_g^+$ electronic state and a 0.3 ns for the lowest triplet Σ state. This value can be compared with the one for K_2 in the first excited singlet electronic state which is 6.6 ps.[8] Even if in these experiments, the Rb_2 dimer is adsorbed on an helium surface, microscopic information on the vibrational relaxation of Rb_2 induced by He could provide some additional insight in understanding the observed decoherence process.

The vibrational quenching mechanism of alkali dimers induced by collisions with helium atoms has been theoretically addressed in the group of Gianturco[9,10] for Li_2 and Cs_2. In particular, the difference on the quenching cross sections for these two extreme cases, the light Li_2 dimer and the heavy Cs_2 one, is explained by the different energy spacing of the vibrational levels, large for Li_2 and small for Cs_2. The mass of Rb_2 would lead to conclude that the results for this dimer should be closer to the Cs_2 results than to the Li_2 ones. However given the extremely shallow Cs_2He potential surface, direct conclusion on the behavior of the quenching in the case of rubidium is not straightforward and calculations are needed.

In the following sections we present the theoretical approach used for the scattering calculations. Then we present both elastic and inelastic rate coefficients of the $Rb_2(v=1,j=0)$ + ^{3,4}He collisions. Finally the details of the bound state determination are presented before concluding remarks.

Scattering calculations

Theory

Quantum calculations of the elastic and inelastic $Rb_2(v=1,j=0)$ + He $\rightarrow$ $Rb_2(v',j')$ + He collision for partial waves with non-zero total angular momentum J have been performed with a time-independent close coupling approach. As in a previous paper,[2] we employed the modified version of the MOLCOL computer code[11] with the resolution of the coupled equations by the Johnson-Manolopoulos[12] log-derivative propagator. It permits to obtain T matrix elements in the space-fixed $|vj\ell JM\rangle$ representation[13] where v and j are the vibrational and rotational quantum numbers of the diatomic, ℓ is the orbital angular momentum of the relative particle, and J and M are the total angular momentum quantum numbers of the atom-molecule system. This code has been modified and extended to determine both bound and scattering states of the complex (see below the section "Bound states").

In this work we are interested in collisions for the initial $(v=1,j=0)$ rovibrational level. We

computed the following rate coefficients :

$$K_{\rm El} = \sum_J K^J_{\rm El} = \frac{\pi\hbar}{\mu k_{10}} \sum_J (2J+1)|T^J_{10J,10J}|^2 \quad (1a)$$

$$K_{\rm Rot} = \sum_J K^J_{\rm Rot} = \frac{\pi\hbar}{\mu k_{10}} \sum_J (2J+1) \sum_{j'\neq 0} \sum_{\ell'} |T^J_{1j'\ell',10J}|^2 \quad (1b)$$

$$K_{\rm Vib} = \sum_J K^J_{\rm Vib} = \frac{\pi\hbar}{\mu k_{10}} \sum_J (2J+1) \sum_{v'\neq 1} \sum_{j'} \sum_{\ell'} |T^J_{v'\ell'l',10J}|^2 \quad (1c)$$

$$K_{\rm In} = \sum_J K^J_{\rm In} = K_{\rm Rot} + K_{\rm Vib}, \quad (1d)$$

where $T^J_{v'j'\ell',vj\ell}$ denotes T matrix elements for a total angular momentum J between the $vj\ell$ and $v'j'\ell'$ channels, $k_{10} = \sqrt{2\mu E_{\rm col}}$ is the initial wave-vector and μ is the reduced mass for the Rb_2 + He system. In these expressions, $K_{\rm El}$ is the elastic rate coefficient, $K_{\rm Rot}$ is the rate for changing the rotational state without modification of the vibrational state, and $K_{\rm Vib}$ is the rate coefficient for changing the vibrational state of the diatomic, with all possible final rotational j' values. Since the initial rotational state is $j = 0$, $K_{\rm Rot}$ is a rate for rotational excitation. In the energy range we considered, the $v = 2$ vibrational level is not accessible energetically and $K_{\rm Vib}$ is thus the rate for relaxation to the ground vibrational state $v' = 0$. Finally, $K_{\rm In}$ is the inelastic rate for the $(v = 1, j = 0)$ rovibrational level.

We included rovibrational states of $^{87}Rb_2$ with $v = 0,\ldots,5$ and $j = 0,2,\ldots,48$ in the close-coupling expansion and we used a propagation distance ranging from 4 to 120 a_0. A discrete variable representation (DVR) with 200 grid points equally spaced between 9 and 30 a_0 has been used to determine the rovibrational states of $^{87}Rb_2$. The rotational constant of $^{87}Rb_2$ is 0.0148 K and the $v = 0 \rightarrow v = 1$ excitation energy is 18.223 K. Eighteen even j rotational levels of the vibrational $v = 0$ ground state lie below the $(v = 1, j = 0)$ level. All the results (elastic and inelastic) which are displayed are converged to graphical accuracy.

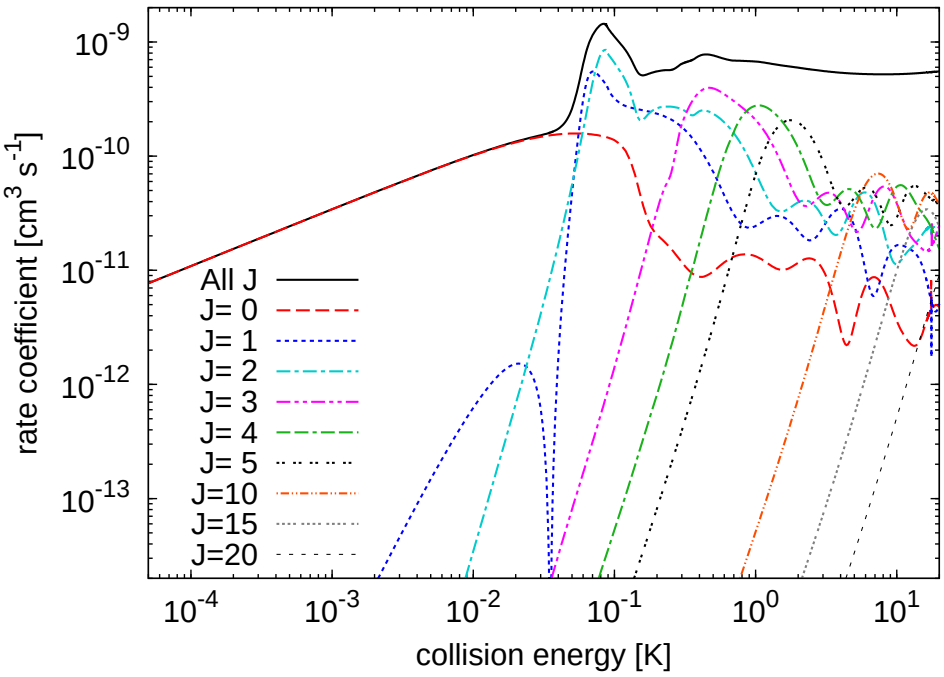

Figure 1: (color) Elastic rate coefficient, $K_{\rm El}$, (black full line) for ^{4}He + ^{87}Rb$_2$ collisions with the initial $v = 1$, $j = 0$ rovibrational state of Rb_2 as a function of the collisional energy in Kelvin. Some relevant partial wave contributions $K^J_{\rm El}$ are shown.

Elastic scattering

Figure 1 shows the elastic rate coefficient $K_{\rm El}$ for ^{4}He. The collision energy $E_{\rm col}$ ranges from 50 microK to 18 K. At the highest collision energies it is necessary to include partial wave contributions up to $J = 20$ to obtain converged rate coefficients. For energies below 20 milliK, the $J = 0$ partial wave is the only one which contributes and the rate coefficient $K_{\rm El}$ increases as $E_{\rm col}^{1/2}$. $K_{\rm El}$ reaches a maximum value of 1.4 10^{-9} cm^{3}s^{-1} at 84 milliK with a main contribution coming from the $J = 1$ and $J = 2$ partial waves.

For scattering by a central potential, the phase-shift δ_ℓ for each value of the orbital angular momentum ℓ follows Wigner threshold laws. For a potential ranging asymptotically as C_n/R^n, the behavior of δ_ℓ when $k \to 0$ reads [14]

$$\delta_\ell \propto k^\alpha, \qquad \text{with } \alpha = \min(2\ell+1, n-2). \tag{2}$$

In the case of He+Rb_2 ($v = 1, j = 0$) scattering, the initial orbital angular momentum ℓ is equal to the total angular momentum J and the above relation can be transposed for the partial elastic rate coefficient $K_{\rm El}^J$ as

$$K_{\rm El}^J \propto E_{\rm col}^{\alpha-\frac{1}{2}} \tag{3}$$

for small collisional energies. When considering a purely C_6/R^6 long range interaction potential, the Wigner threshold laws thus predict that the partial elastic rate $K_{\rm El}^J$ should increase as $E_{\rm col}^{1/2}$ for $J = 0$ and as $E_{\rm col}^{5/2}$ for $J = 1$. The computed rate coefficients follow indeed very well this behavior. For $J \geq 2$ the computed rate coefficients shown in Figure 1 vary as $E_{\rm col}^{\eta}$ where $\eta \simeq 3.9$ instead of $E_{\rm col}^{7/2}$ as expected from Wigner threshold law with $n = 6$ and $\ell \geq 2$. This behavior can be explained by the fact that the interaction potential as a function of the Jacobi Rb_2-He distance R is not strictly speaking C_6/R^6 at large distances but the sum of two $C_6/R_{\rm RbHe}^6$ rubidium-helium potential terms. Indeed in the fitting procedure of the Rb_2-He interaction potential[2] a many-body decomposition has been used. Because the 3-body term vanishes at large Rb_2-He distances, the full potential resumes to the two 2-body terms between the helium and each rubidium atom for large R values. Figure 2 illustrates the deviation of the Rb_2-He isotropic component of the interaction potential from a pure C_6/R^6 behavior. The relative deviation between the averaged potential, $(V(R,\theta = 0) + 2\,V(R,\theta = 90))/3$, relevant for the initial $j = 0$ state of the Rb_2 molecule and a pure C_6/R^6 is given in percent as a function of the distance R in logscale. For large distances, the largest deviations are observed for the linear ($\theta = 0$) approach. At a distance of $R = 120\ a_0$, the actual interaction potential deviates from a C_6/R^6 behavior by 5% for a linear approach of the helium atom. The corresponding potential value for this geometry is around -10 microK. The C_6/R^6 behavior is however valid at very large Rb_2-He distances and extremely small energies. For example at $R = 350\,a_0$, the deviation to the C_6/R^6 behavior drops to 0.5% with potential values of the order of -10 nanoK. These large distances take importance for energies which are lower than the ones presented on Figure 1 for these $J > 2$ partial waves and the corresponding rate coefficients lie below 10^{-14} $\rm cm^3 s^{-1}$.

Figure 3 presents results for the lighter ^{3}He isotope. Calculations with J up to 20 have also

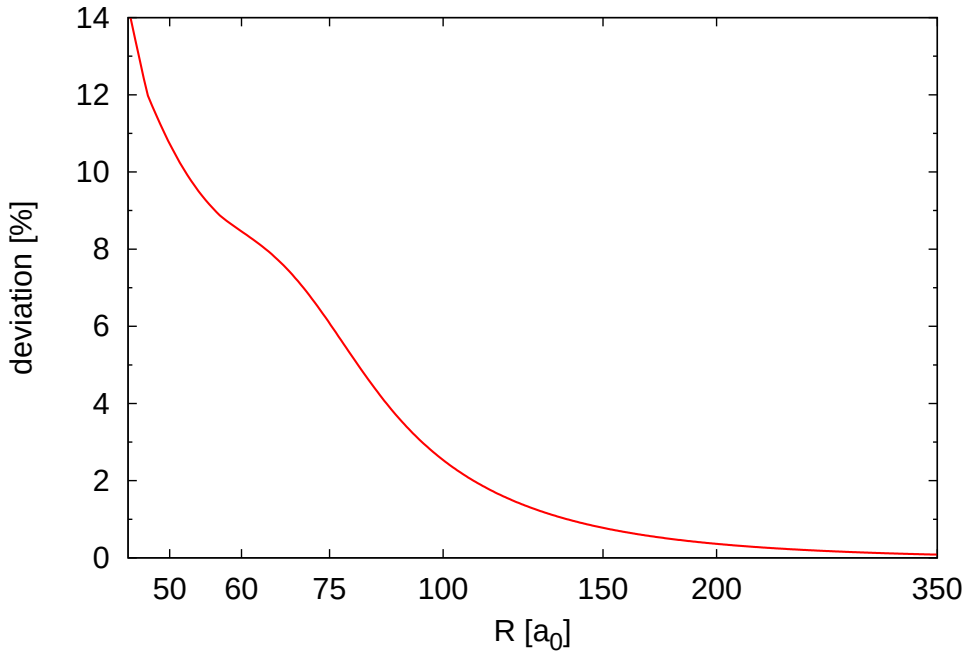

Figure 2: Deviation in % of the isotropic component of the Rb_2He interaction potential from a C_6/R^6 behavior as a function of the Rb_2-He distance in bohr. See text for details.

been found necessary to converge the rate coefficients in the considered energy domain. The $J = 0$ contribution is dominant below 0.7 milliK. This is much lower than for ^{4}He because of the very strong resonance in the $J = 1$ partial wave that occurs at 3.5 milliK where the rate coefficient reaches 4 10^{-9} cm^3s^{-1}. The importance of the $J = 1$ partial wave contribution for this isotope renders the conclusions based on the $J = 0$ partial wave[2] rather limited. The applicability of the Wigner threshold laws for $J = 0$ and $J = 1$ and the discussion for larger J values (Figure 3) is similar to the ^{4}He case.

Vibrational relaxation and inelastic scattering

The understanding of the vibrational damping mechanism of Rb_2 on the surface of helium nanodroplets could benefit from information on the vibrational relaxation rate coefficients K_{Vib}. Figures 4 and 5 show K_{Vib} for ^{4}He and ^{3}He in the same collisional energy range as above. For both helium isotopes we needed partial waves up to $J = 15$ to get converged rate coefficients. At low

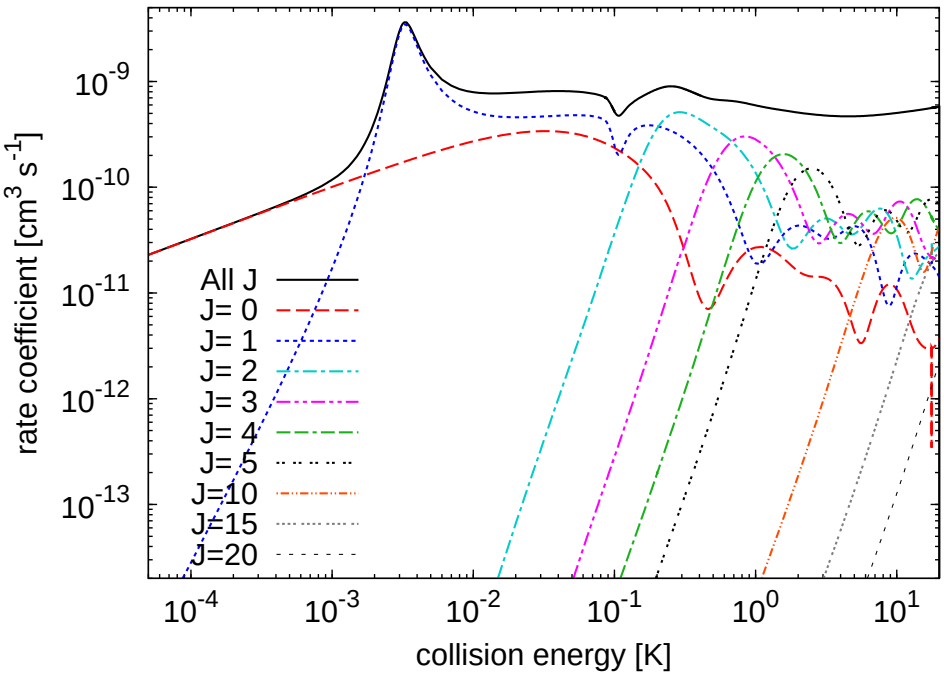

Figure 3: (color) Elastic rate coefficient, $K_{\rm El}$, (black full line) for ^{3}He + ^{87}Rb$_2$ collisions with the initial $v = 1$, $j = 0$ rovibrational state of Rb_2 as a function of the collisional energy in Kelvin. Some relevant partial wave contributions $K^J_{\rm El}$ are shown.

collision energies, Wigner threshold laws predict that the partial $K^J_{\rm Vib}$ rate coefficients vary as

$$K^J_{\rm Vib} \propto E^J_{\rm col}. \tag{4}$$

This behavior is valid below 10 milliK for the $J = 0$ partial wave contribution which is nearly constant for both ^{3}He and ^{4}He. We found numerically that the contribution of each relevant partial wave varies as $E^J_{\rm col}$ at low energy.

The $J = 1$ partial wave has a strong influence on the global rate coefficient at energies which lie in the 0.5 - 100 milliK range for ^{4}He and in the 1 microK - 10 milliK range for ^{3}He. This is due to resonance features in the $J = 1$ partial wave that appear as a peak for both isotopes. It occurs at 63 milliK with a value of 1.42 10^{-11} cm^{3}s^{-1} for ^{4}He and at 3.2 milliK with a value of 2.76 10^{-10} cm^{3}s^{-1} for ^{3}He. We analyzed the evolution of the energy position of these two $J = 1$ peaks as a function of the helium mass and we found that they are not related. When increasing the

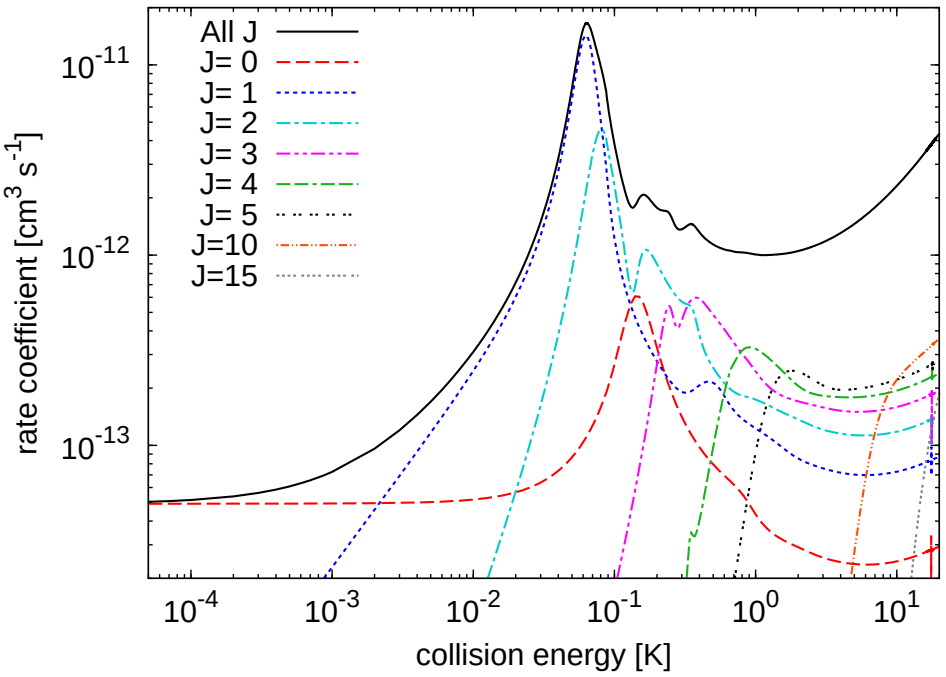

Figure 4: (color) Vibrational relaxation rate coefficient, K_{Vib}, (black full line) for ^{4}He + ^{87}Rb$_2(v = 1, j = 0)$ collisions as a function of the collisional energy in Kelvin. Some relevant partial wave contributions K^J_{Vib} are shown.

helium mass from ^{3}He to ^{4}He the first resonance of ^{3}He at 3.2 milliK goes below the $(v = 1, j = 0)$ threshold and the second resonance which appears as a little hump at 100 milliK correlates to the 63 milliK peak seen in ^{4}He. In Figure 5 another resonance feature is present for the $J = 2$ partial wave contribution. It shows up as a peak at 0.7 milliK which amounts to 1.38 10^{-13} cm^{3}s^{-1} in $K^{J=2}_{\mathrm{Vib}}$. Assuming that the resonance features are associated with an helium atom stuck for some time around Rb$_2$ and given that in our previous study[2] we showed that the vibration of Rb$_2$ has a very small effect on the vibrationally averaged Rb$_2(v)$-He interaction potential for low vibrational v states we can conclude that the two low energy peaks observed on Figure 5 for the $J = 1$ and $J = 2$ partial waves are related to ^{87}Rb$_2{}^4$He bound states. If one transposes these $v = 1$ findings to the case of the $v = 0$ ground vibrational state of Rb$_2$, the increase of mass from ^{3}He to ^{4}He would be responsible for the modification of quasi-bound states of ^{87}Rb$_2{}^3$He to the bound states of ^{87}Rb$_2{}^4$He labelled as 1^- and 2^+ (see below Table 1 and the discussion in section "Bound states"). For both isotopes the total vibrational relaxation rate coefficient is affected by these resonances in

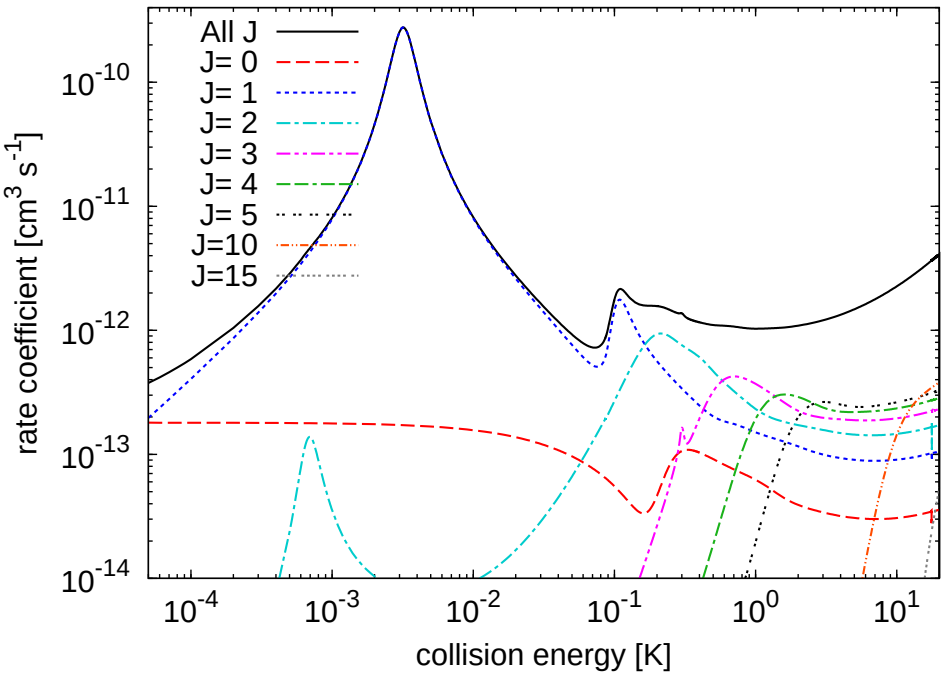

Figure 5: (color) Vibrational relaxation rate coefficient, $K_{\rm Vib}$, (black full line) for ^{3}He + ^{87}Rb$_2(v = 1, j = 0)$ collisions as a function of the collisional energy in Kelvin. Some relevant partial wave contributions $K^J_{\rm Vib}$ are also shown.

the $J = 1$ partial wave. The effect is about ten times larger for the lighter helium isotope.

Figure 6 shows the inelastic rate coefficients $K_{\rm In}$, for both helium isotopes. In the present collisional energy range the inelastic rate coefficients lie below the elastic ones shown in Figures 1 and 3. Due to the definition of $K_{\rm Vib}$ given in Eq. (1) and to the initial state considered in this work, $K_{\rm In}$ is identical to $K_{\rm Vib}$ below the opening of the $(v = 1, j = 2)$ level at 90 mk. Thus the resonance features detailed above for $K_{\rm Vib}$ are the same in Figure 6. For collisional energies above 90 milliK, vibrational relaxation turns out to be much less efficient than rotational excitation and $K_{\rm In} \simeq K_{\rm Rot} \gg K_{\rm Vib}$. For both isotopes, $K_{\rm Vib}$ amounts to a few 10^{-12} cm^{3}s^{-1} whereas $K_{\rm In}$ reaches 10^{-10} cm^{3}s^{-1}. For ^{3}He the magnitude of the resonance at 3.2 milliK is such that the vibrational relaxation rate coefficient is as important as the rotational excitation observed for higher collision energies.

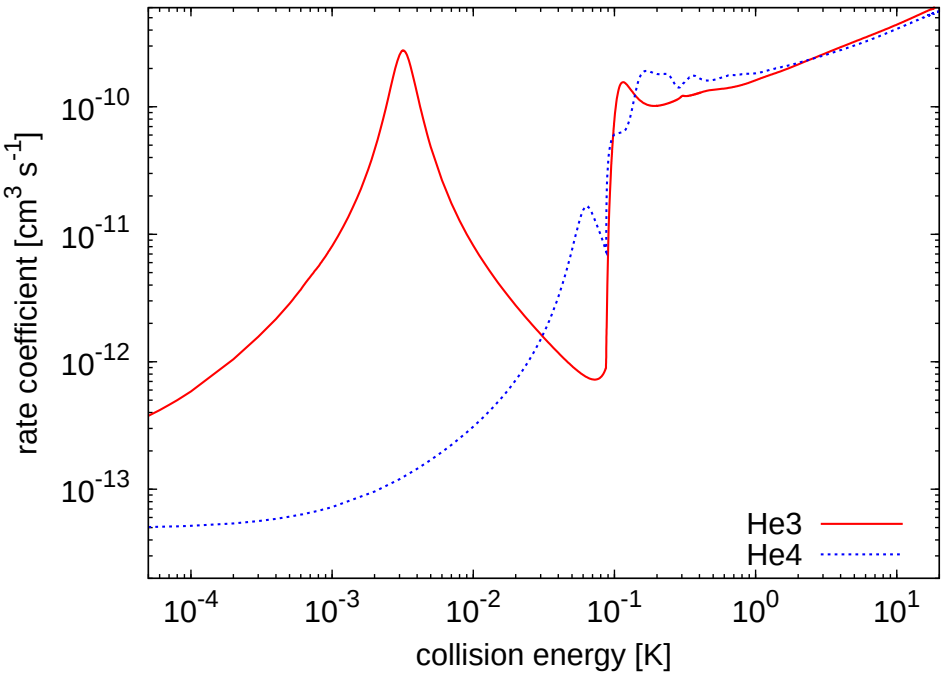

Figure 6: (color) Inelastic rate coefficients, K_{In}, for ^{4}He + ^{87}Rb$_2(v=1, j=0)$ and ^{3}He + ^{87}Rb$_2(v=1, j=0)$ collisions as a function of the collision energy in Kelvin.

Bound states

An extension of our scattering code has been done to enable bound state calculations. To this end we developped a high-order finite element method to represent the $F^J_{vj\ell}(R)$ radial functions in the close coupling expansion. The total domain of atom-diatom Jacobi distances R is split into elements in which the radial wavefunctions are expanded over high degree polynomials. This procedure permits to build the hamiltonian matrix. Radial wavefunctions are then enforced to vanish at both endpoints of the domain and bound states are obtained by diagonalization of the hamiltonian matrix. Alternative boundary conditions, for example R-matrix boundary conditions, can be used at the right endpoint of the integration domain to compute the continuum states. They are determined at each energy by solving a real symmetric linear equations system and are further used to generate the scattering states with the usual asymptotic behaviour. We tested the stability and accuracy of this method on several model systems and reproduced accurately the results presented in the previous section. We also considered the CO-He complex bound states and obtained good

agreement with Peterson and Mc Bane[15] who used the BOUND program.[16,17]

In the case of the Rb_2-He complex, an extended total R-domain ranging from 4 a_0 to 200 a_0 has been used to ensure that the very diffuse character of the bound states is properly represented. The total range was divided into 49 elements of equal width in which the radial wavefunction was expanded on polynomials of degree 20. Rovibrational states with $v = 0, 1$ and even $j \leq 24$ have been used in the close-coupling expansion. The resulting hamiltonian matrix is of order 25974. It is very sparse with a filling factor equal to $9\ 10^{-4}$. The eigenvalues and eigenvectors were obtained with a sparse real symmetric matrix diagonalizer based on the FEAST algorithm.[18]

The energy levels are summarized in Table 1 for both isotopes. We found that the lighter $^{87}Rb_2{}^3He$ complex has only one bound state with $J = 0$ and that the $^{87}Rb_2{}^4He$ complex has four bound states, one for each partial wave $J = 0$ and 1 and two for $J = 2$. Our calculations show that there is only one bound state for $J = 0$ for both helium isotopes as already concluded in an indirect way for ^3He in a previous paper.[2] The four levels of the heavier complex have been represented schematically on Figure 7. They are denoted by their J^Π symmetry quantum numbers where $\Pi = (-1)^{j+\ell}$ denotes the parity of the complex. In addition to the energy, Table 1 presents the $vj\ell$ channels on which the wave-function has a non-negligible amplitude. This amplitude is characterized by the partial norm (*PN*) of the wavefunction in a given channel $vj\ell$, defined by the expression:

$$PN^J_{vj\ell} = \int_0^\infty |F^J_{vj\ell}(R)|^2\, dR. \tag{5}$$

The sum of *PN* values over all $vj\ell$ channels is 1 because the wavefunction is normalized to unity.

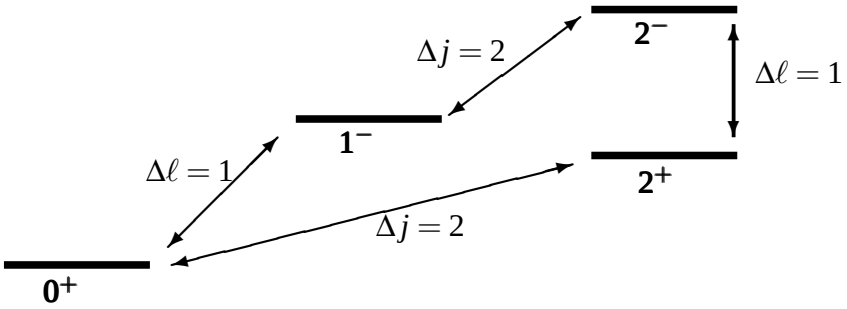

Figure 7: Schematic representation of the four $^{87}Rb_2{}^4He$ bound state energy levels denoted by their J^Π label.

Table 1: Bound state energy levels in milliK for the $^{87}Rb_2{}^4He$ and $^{87}Rb_2{}^3He$ complexes. The zero of energy is taken for separated $^{87}Rb_2(v=0,j=0)$ and He systems. The partial norm *PN* illustrates the expansion of the eigenfunctions on $vj\ell$ channels. See text for the definition. Only *PN* values larger than 1% have been indicated in the table.

	J	Π	E	v,j,ℓ	*PN* in %
$^{87}Rb_2{}^4He$	0	+	-205.0	$0,0,0$	85
				$0,2,2$	13
				$0,4,4$	2
$^{87}Rb_2{}^4He$	1	-	-112.8	$0,0,1$	77
				$0,2,1$	16
				$0,2,3$	4
				$0,4,3$	2
$^{87}Rb_2{}^4He$	2	+	-119.2	$0,2,0$	83
				$0,4,2$	6
				$0,0,2$	5
				$0,2,2$	4
				$0,2,4$	1
$^{87}Rb_2{}^4He$	2	-	-45.5	$0,2,1$	94
				$0,2,3$	4
				$0,4,3$	2
$^{87}Rb_2{}^3He$	0	+	-87.2	$0,0,0$	93
				$0,2,2$	6

Table 1 and Figure 7 show that the energy ordering of the levels while increasing the total angular momentum J from 0 to 2 is non monotonous because the energy of the 2^+ level lies below the one of the 1^- level. The expansion of the corresponding eigenfunctions shows that from 0^+ to 2^+ the main channel shifts from $j=0$ to $j=2$ while for the 0^+ to 1^- it shifts from $\ell=0$ to $\ell=1$. These shifts are denoted by Δj and $\Delta\ell$ on Figure 7. For an isolated Rb_2 diatomic, the $j=2$ level lies 90 milliK above the $j=0$ ground level. For the Rb_2He complex, the energy difference $E(2^+)-E(0^+)$ is roughly the same with a 85.8 milliK value and we can assume that this state represents a rotating Rb_2 molecule with a surrounding attached He atom whose mass contributes to the lowering of the effective rotational constant of Rb_2. Because the dominant channel has also

an $\ell = 0$ value the helium density of this 2^+ state should be similar to the one of the 0^+ ground state. For the 1^- state, we expect a strong modification of the helium probability density with respect to 0^+ because of the $\ell = 1$ dominant character of the wave-function. Thus the energy difference $E(1^-) - E(0^+) = 92.2$ milliK is not related to the rotation of the Rb_2 which stays predominantly in the $j = 0$ channel.

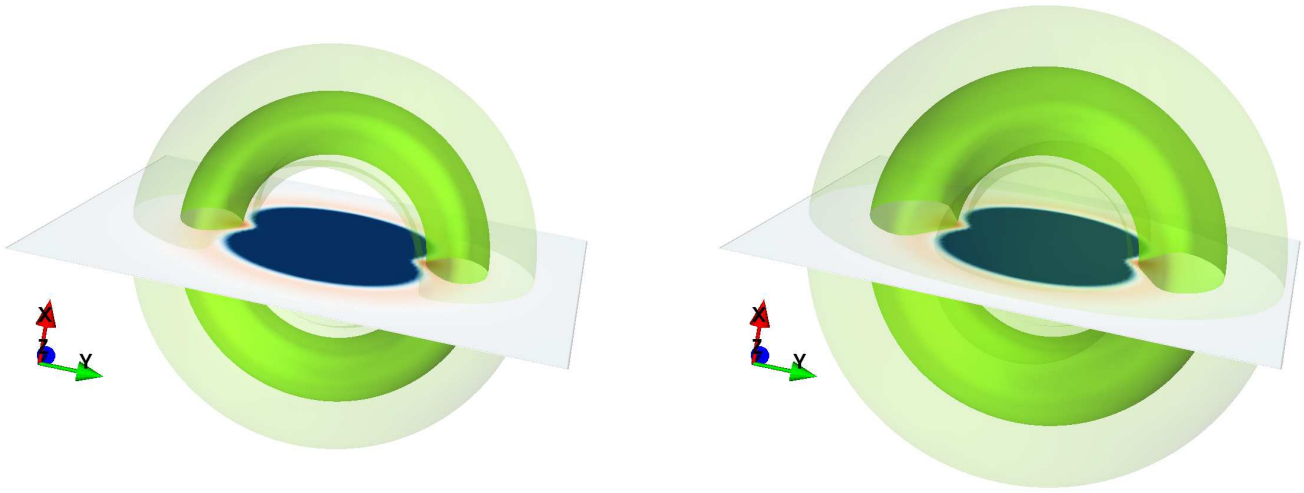

Figure 8: (color) Iso-density surfaces of the $J = 0$ eigenfunctions for $^{87}Rb_2{}^4He$ (left panel) and $^{87}Rb_2{}^3He$ (right panel). The volume inside the dark green isosurface contains 30% of the probability to find helium and the one inside the light green surface 70%. A cut of the Rb_2 He potential energy surface is given in the *zy* plane with color codes such as blue is repulsive, red is attractive and white corresponds to the asymptotic limit. The *z* direction lies along the Rb_2 axis.

Figure 8 presents the probability densities for the $J = 0$ eigenfunctions of $Rb_2{}^4He$ and $Rb_2{}^3He$ together with a cut of the interaction potential. It shows iso-density surfaces corresponding to the expansion onto the $v = 0$ vibrational state of the Rb_2 dimer. The iso-density surfaces were chosen such that they contain a volume corresponding to 30% and 70% of the probability to find helium. A cut of the potential energy surface is also presented in the *zy* plane as an eye guide. We used the equilibrium Rb_2 distance to produce the color map of the interaction potential. The repulsive part of the potential is clearly seen in blue surrounded by a reddish attractive part. The global minimum of the surface[2] corresponds to a T-shape geometry with a distance He-Rb_2 of 11.9 a_0 and has

a depth of 3.73 K with respect to the Rb_2 + He asymptote. The asymptotic potential value is represented in white. The same scale is used for both helium isotopes underlying the more diffuse character of the wavefunction of the lighter helium isotope (right panel). The two isosurfaces for ^{4}He are torii surrounding the waist of the Rb_2 molecule. The dark green isosurface for ^{3}He has the same torus shape. However the light green isosurface for ^{3}He is split into two parts: an outer prolate ellipsoid and an inner peanut. The inner peanut follows the repulsive part of the interaction potential seen in dark blue in the figure. The density is maximum on a circle of radius 14.4 a_0 for ^{4}He and 15 a_0 for ^{3}He lying in the *xy* plane of the Rb_2 waist. It decreases to a small but non-zero value when going along the Rb_2 axis as seen in the figure for ^{3}He and in quantum Monte Carlo studies.[19,20]

The $J = 0$ ground state energy can be compared with the published[19,20] ground state energy of $^{85}Rb_2{}^4$He. These calculations were performed within the rigid rotor approximation and used a quantum Monte Carlo approach. A value of -192.9 ± 0.4 milliK was obtained[19] while a slightly higher value -172.2 ± 0.4 milliK is found by Gianturco and co-workers[20] on an alternative potential energy surface. Direct comparison with the value given in Table 1 is to be avoided given that in the present work the vibration of Rb_2 is included and more important that the above studies concern $^{85}Rb_2$.

Conclusions

In this work, we have studied the vibrational relaxation of $^{87}Rb_2(v = 1, j = 0)$ in its ground triplet state induced by collisions with ^{3}He and ^{4}He isotopes in the cold and ultra cold regimes. Both elastic and inelastic rate coefficients have been determined for collisional energies ranging from 10 microK to 10 K. We also determined all the bound states of $^{87}Rb_2{}^3$He and $^{87}Rb_2{}^4$He with even Rb atom permutation symmetry. For that purpose we have developed a new code that generates both scattering states and bound states. It relies on a high order finite element method to represent the radial functions in the close coupling expansion.

We found that vibrational relaxation is very efficient at low collisional energies for both helium isotopes due to a strong resonance feature in the $J = 1$ partial wave. Nevertheless the elastic rate stays above the inelastic rate in the considered energy domain. A detailed analysis of the behavior at very small energies of the partial wave contributions to the elastic rates demonstrates the influence of the asymptotic R^{-6} potential for $J \geq 2$.

$^{87}Rb_2{}^3He$ supports only one bound state with $J^\Pi = 0^+$ symmetry. $^{87}Rb_2{}^4He$ supports a total of four bound states, one for each symmetry $J^\Pi = 0^+, 1^-, 2^+$ and 2^-. The non monotonous energy ordering as a function of J has been analyzed through the expansion of the bound state eigenfunctions on the $vj\ell$ channels. The $J^\Pi = 0^+$ eigenfunctions for both helium isotopes show both a localized density around the waist of Rb_2 and a diffuse but non-zero helium density along the Rb_2 axis.

In the present work we did not take into account hyperfine and spin rotation terms in the Rb_2 molecule. However a detailed spectroscopic analysis of $^{87}Rb_2$ in the lowest triplet state[21] has shown their importance. These terms have been included in the rotational relaxation studies of Cs_2-He and of Li_2-He by Gianturco and co-workers.[22,23] Work dedicated to assess their role in the collisional observables for Rb_2-He is in progress. Another limitation of the present results is the exclusive use of the low $v = 1$ vibrational state of Rb_2 as the initial state. The effect of low vibrationally excited states up to $v = 4$ has been found to be small in the $J = 0$ partial wave.[2] Preliminary calculations for $J > 0$ showed also a small effect on low vibrationally excited states. However rate coefficients for highly excited states close to the dissociation limit might be strongly affected. Analysis of $Rb_2(v, j = 0)$ + He scattering with a large v could bring a better understanding of the relaxation process observed in pump-probe experiments on helium clusters. Moreover information about scattering from $Rb_2(v, j > 0)$ would allow to discuss the efficiency of buffer gas cooling[24] for this high spin alkali dimer. To our kwnowlege this technique has not yet been employed for alkali dimers. Finally, a more refined analysis of the helium density for bound states with $J > 0$ is needed to better understand the energy spectrum of $Rb_2{}^4He$.

Acknowledgments

This work has been supported by the Région Bretagne via the project CREATE “4023-HELIUM” and by the Agence Nationale de la Recherche via the projects “DYNHELIUM” and “COLORI”. The authors thank A. Simoni for fruitful discussions.

References

[1] Krems, R.; Friedrich, B.; Stwalley, W. C. *Cold Molecules: Theory, Experiment, Applications*; CRC press, 2009.

[2] Guillon, G.; Viel, A.; Launay, J. Full dimension Rb_2He ground triplet potential energy surface and quantum scattering calculations. *J. Chem. Phys.* **2012**, *136*, 174307–1–7.

[3] Toennies, J. P.; Vilesov, A. F. Superfluid helium droplets: a uniquely cold nanomatrix for molecules and molecular complexes. *Angew. Chem. Int. Ed.* **2004**, *43*, 2622–2648.

[4] Stienkemeier, F.; Lehmann, K. K. Spectroscopy and dynamics in helium nanodroplets. *J. Phys. B* **2006**, *39*, R127–R166.

[5] Brühl, F. R.; Miron, R. A.; Ernst, W. E. Triplet states of rubidium dimers on helium nanodroplets. *J. Chem. Phys.* **2001**, *115*, 10275–10281.

[6] Higgins, J.; Callegari, C.; Reho, J.; Stienkemeier, F.; Ernst, W. E.; Gutowski, M.; Scoles, G. Helium cluster isolation spectroscopy of alkali dimers in the triplet manifold. *J. Phys. Chem. A* **1998**, *102*, 4952–4965.

[7] Grüner, B.; Schlesinger, M.; Heister, P.; Strunz, W. T.; Stienkemeier, F.; Mudrich, M. Vibrational relaxation and decoherence of Rb_2 attached to helium nanodroplets. *Phys. Chem. Chem. Phys.* **2011**, *13*, 6816–6826.

[8] Schlesinger, M.; Mudrich, M.; Stienkemeier, F.; Strunz, W. Evidence for Landau’s critical

velocity in superfluid helium nanodroplets from wave packet dynamics of attached potassium dimers. *Chem. Phys. Letters* **2010**, *490*, 245–248.

[9] Bovino, S.; Bodo, E.; Yurtsever, E.; Gianturco, F. A. Vibrational cooling of spin-stretched dimer states by He buffer gas: quantum calculations for $Li_2(a^3\Sigma_u^+)$ at ultralow energies. *J. Chem. Phys.* **2008**, *128*, 224312–1–6.

[10] Caruso, D.; Tacconi, M.; Yurtsever, E.; Bovino, S.; Gianturco, F. A. Quenching vibrations of cesium dimers by He at low and ultralow temperatures: quantum dynamical calculations. *Eur. Phys. J. D.* **2011**, *65*, 167–175.

[11] Flower, D. R.; Bourhis, G.; Launay, J.-M. MOLCOL: a program for solving atomic and molecular collision problems. *Comp. Phys. Com.* **2000**, *131*, 187–201.

[12] Manolopoulos, D. E. An improved log-derivative method for inelastic scattering. *J. Chem. Phys.* **1986**, *85*, 6425–6429.

[13] Arthurs, A. M.; Dalgarno, A. The Theory of Scattering by a Rigid Rotator. *Proc. Roy. Soc. A* **1961**, *256*, 540–551.

[14] Weiner, J.; Bagnato, V. S.; Zilio, S.; Julienne, P. S. Experiments and theory in cold and ultracold collisions. *Rev. Mod. Phys.* **1999**, *71*, 1–85.

[15] Peterson, K. A.; McBane, G. C. A hierarchical family of three-dimensional potential energy surfaces for He-CO. *J. Chem. Phys.* **2005**, *123*, 084314–1–15.

[16] Hutson, J. M. Coupled channel methods for solving the bound-state Schrœdinger equation. *Comp. Phys. Com.* **1994**, *84*, 1–18.

[17] Hutson, J. M. BOUND computer code, Version 5, distributed by Collaborative Computational Project No. 6 of the Science and Engineering Research Council (UK 1993).

[18] Polizzi, E. Density-matrix-based algorithm for solving eigenvalue problems. *Phys. Rev. B* **2009**, *79*, 115112–1–6.

[19] Guillon, G.; Zanchet, A.; Leino, M.; Viel, A.; Zillich, R. E. Theoretical study of Rb_2 in He_n: potential energy surface and Monte Carlo simulations. *J. Phys. Chem. A* **2011**, *115*, 6918–6926.

[20] Rodríguez-Cantano, R.; Lopez-Durán, D.; González-Lezana, T.; Delgado-Barrio, G.; Villarreal, P.; Yurtsever, E.; Gianturco, F. A. Spin-Polirazed Rb_2 interacting with bosonic He atoms: potential energy surface and quantum structures of small clusters. *J. Phys. Chem. A* **2012**, *116*, 2394–2404.

[21] Strauss, C.; Takekoshi, T.; Lang, F.; Winkler, K.; Grimm, R.; Denschlag, J. H.; Tiemann, E. Hyperfine, rotational, and vibrational structure of the $a^3\Sigma_u^+$ state of $^{87}Rb_2$. *Phys. Rev. A* **2010**, *82*, 052514–1–12.

[22] Caruso, D.; Tacconi, M.; Yurtsever, E.; Gianturco, F. A. Quenching of internal rotations versus collisional cooling at ultralow energies for weakly interacting partners: $Cs_2(^3\Sigma_u^+)$ with ^{3,4}He. *Phys. Rev. A* **2010**, *81*, 042710–1–9.

[23] González-Sánchez, L.; Bodo, E.; Gianturco, F. A. Collisional quenching of rotations in lithium dimers by ultracold helium: the $Li_2(a^3\Sigma_u^+)$ and $Li_2^+(X^2\Sigma_g^+)$ targets. *J. Chem. Phys.* **2007**, *127*, 244315–1–8.

[24] Campbell, W. C.; Doyle, J. M. In *Cold Molecules: Theory, Experiment, Applications*; Krems, R., Friedrich, B., Stwalley, W. C., Eds.; CRC press, 2009; pp 273–508.